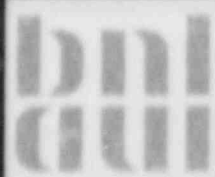


RELIABILITY ASSESSMENT OF INDIAN POINT UNIT 3 CONTAINMENT STRUCTURE

J. Kawakami, H. Hwang, M.T. Chang, and M. Reich

Date Published — January 1984

STRUCTURAL ANALYSIS DIVISION
DEPARTMENT OF NUCLEAR ENERGY, BROOKHAVEN NATIONAL LABORATORY
UPTON, LONG ISLAND, NEW YORK 11973



Prepared for
U.S. Nuclear Regulatory Commission
Washington, D.C. 20555

RELIABILITY ASSESSMENT OF INDIAN POINT UNIT 3 CONTAINMENT STRUCTURE

J. Kawakami, H. Hwang, M.T. Chang, and M. Reich

Manuscript Completed - October 1983
Date Published - January 1984

STRUCTURAL ANALYSIS DIVISION
DEPARTMENT OF NUCLEAR ENERGY
BROOKHAVEN NATIONAL LABORATORY
UPTON, LONG ISLAND, NEW YORK 11973

PREPARED FOR
UNITED STATES NUCLEAR REGULATORY COMMISSION
WASHINGTON, D.C. 20555
CONTRACT NO. DE-AC02-76CH00016
FIN A-3226

NOTICE

This report was prepared as an account of work sponsored by an agency of the United States Government. Neither the United States Government nor any agency thereof, or any of their employees, makes any warranty, expressed or implied, or assumes any legal liability or responsibility for any third party's use, or the results of such use, of any information, apparatus, product or process disclosed in this report, or represents that its use by such third party would not infringe privately owned rights.

The views expressed in this report are not necessarily those of the U.S. Nuclear Regulatory Commission.

Available from
GPO Sales Program
Division of Technical Information and Document Control
U.S. Nuclear Regulatory Commission
Washington, D.C. 20555
and
National Technical Information Service
Springfield, Virginia 22161

Abstract

In the current design criteria, the load combinations specified for design of concrete containment structures are in the deterministic formats. However, by applying the probability-based reliability method developed by BNL to the concrete containment structures designed according to the criteria, it is possible to evaluate the reliability levels implied in the current design criteria. For this purpose, the reliability analysis is applied to the Indian Point Unit No. 3 containment.

The details of the containment structure such as the geometries and the rebar arrangements, etc., are taken from the working drawings and the final safety analysis reports. Three kinds of loads are considered in the reliability analysis. They are, dead load (D), accidental pressure due to a large LOCA (P), and earthquake ground acceleration (E). Reliability analysis of the containment subjected to all combinations of loads is performed. The results are presented in this report.

Table of Contents

	<u>Page</u>
Abstract.....	iii
List of Tables.....	vii
List of Figures.....	viii
Acknowledgement.....	ix
1. INTRODUCTION.....	1
2. CONTAINMENT DESCRIPTION.....	1
2.1 Geometry.....	1
2.2 Design Loads.....	2
2.3 Rebar Arrangements.....	3
3. CONTAINMENT MODELLING.....	4
4. MATERIAL PROPERTIES.....	5
5. PROBABILISTIC MODELS FOR LOADS.....	6
5.1 Dead Load.....	6
5.2 Accidental Pressure.....	6
5.3 Earthquake Ground Acceleration.....	7
6. FINITE ELEMENT ANALYSIS OF THE CONTAINMENT.....	9
6.1 Static Analysis.....	10
6.2 Dynamic Analysis.....	10
7. LIMIT STATE FOR THE CONTAINMENT.....	10

Table of Contents (Cont'd)

	<u>Page</u>
8. RELIABILITY ANALYSIS RESULTS.....	11
8.1 Dead Load and Accidental Pressure (D+P).....	12
8.2 Dead Load and Earthquake Ground Acceleration (D+E).....	12
8.3 Dead Load, Earthquake Ground Acceleration and Accidental Pressure (D+E+P).....	13
8.4 Overall Limit State Probability.....	14
9. RESULTS FOR DIFFERENT LIMIT STATE.....	14
10. CONCLUDING REMARKS.....	15
References.....	16

LIST OF TABLES

<u>Table</u>		<u>Page</u>
1	Cylinder Reinforcement.....	18
2	Dome Reinforcement.....	19
3	Load Parameters.....	20
4	Stresses Due to Dead Load.....	21
5	Stresses Due to Unit Pressure.....	22
6	Natural Frequencies.....	23
7	Coordinates of Limit State Surface (Element 289 - 312, Local X-Direction).....	24
8	Conditional Limit State Probability $p^{(D+P)}$	25
9	Conditional Limit State Probability $p^{(D+E)}$	26
10	Conditional Limit State Probability $p^{(D+E+P)}$	27
11	Lifetime Limit State Probabilities (Based on Linear Stress Distribution).....	28
12	Lifetime Limit State Probabilities (Based on Nonlinear Stress Distribution).....	29

LIST OF FIGURES

<u>Figure</u>		<u>Page</u>
1	Cross Section of Containment (Section A-A).....	30
2	Cross Section of Containment (Section B-B).....	31
3	Sketch of Containment Structure.....	32
4	Time Histories of Design Pressure and Temperature.....	33
5	Typical Rebar Arrangement for Cylindrical Wall.....	34
6	Meridional Rebar Arrangement (Dome).....	35
7	Three-Dimensional Model for Containment.....	36
8	Side View of Containment Model.....	37
9	Top View of Containment Model.....	38
10	Cross Section of Containment Model.....	39
11	Three-Dimensional Sketch of Mode Shapes (Modes 1 and 2).....	40
12	Three-Dimensional Sketch of Mode Shapes (Modes 15 and 16).....	41
13	Limit State Surface (Elements 289 - 312, Local X-Direction).....	42
14	Conditional Limit State Probability Distributions.....	43

ACKNOWLEDGEMENTS

The authors wish to express their appreciation to Mr. H. Ashar of the Nuclear Regulatory Commission for his advice and support during various phases of this study. The authors also wish to thank the Power Authority of the State of New York and United Engineers and Contractors for providing the drawings and test data.

Thanks are due to Mr. D. Suwannakate for preparing the figures and to Ms. Diana Votruba for the typing of this manuscript.

1. INTRODUCTION

Concrete containment structures in the United States are currently designed according to the ASME code¹ and other supplementary requirements such as Standard Review Plan (SRP)², etc. The load combinations specified in these criteria are in the deterministic format and the reliability levels implied in the load combinations are not stated explicitly. For the safety evaluation of the nuclear structures, however, it is important to know these reliability levels.

The Structural Analysis Division of Brookhaven National Laboratory (BNL) has been developing a probability-based reliability analysis methodology for nuclear structures, particularly for concrete containment structures.³⁻⁵ An important feature of this methodology is the incorporation of finite element analysis and random vibration theory. By utilizing this method, it is possible to evaluate the safety of nuclear structures under various static and dynamic loads in terms of limit state probability.

By applying the reliability analysis method to the concrete containment structures designed according to the criteria mentioned above, it is possible to evaluate the reliability levels implied in the current design criteria. For this purpose, the reliability analysis is applied to the Indian Point Unit No. 3 containment structure. The results of the reliability analysis are presented in this report.

2. CONTAINMENT DESCRIPTION

2.1 Geometry

The Indian Point Unit No. 3 nuclear power plant employs a pressurized water reactor nuclear steam supply system furnished by Westinghouse Electric Corporation. The containment structure completely encloses the entire reactor and reactor coolant system and ensures that essentially no leakage of radioactive materials to the environment would result even if gross failure of the reactor coolant system were to occur. The structure also provides biological shielding for normal and accident situations.

Two typical cross-sections of the containment are shown in Figs. 1 and 2. The reactor containment structure consists of a vertical right cylinder with a hemispherical dome on the top. The cylinder-dome system is built on a base-mat with thickness 9'-0". Thus, the cylinder-dome system is considered to be fixed at the base in the present analysis for simplicity. The concrete containment structure is illustrated in Fig. 3. The thickness of the dome is equal to 3'-6", whereas the thickness of the cylindrical wall is 4'-6". The inside radius of the dome and the cylinder is equal to 67'-6". The height of the cylindrical wall is 148'-0" and the total height of the containment is 219'-0". These dimensions are also shown in Fig. 3.

2.2 Design Loads

The containment structure is subjected to various static and dynamic loads during its lifetime. In this study, only three types of loads are taken into consideration. They are: dead load, accidental internal pressure and earthquake ground acceleration. From reviewing the drawings and the Final Safety Analysis Report (FSAR)⁷, it is found that there is no live load acting on the containment structure.

The dead loads arise mainly from the weights of the dome and the cylinder. The weight density of the reinforced concrete is taken to be 150 lb/ft³. The accidental internal pressure is assumed to be caused by a large Loss of Coolant Accident (LOCA). The time history of the accidental pressure is shown in Fig. 4, which is taken from FSAR. The accidental pressure is considered as a quasi-static load and is uniformly distributed on the containment wall. The design value of the pressure is 47 psi.

From FSAR, the design value of the ground acceleration for the Operational Basis Earthquake (OBE) is determined to be 0.1 g applied horizontally and 0.05 g applied vertically. Additionally, the ground acceleration for the Design Basis Earthquake (DBE) is determined to be 0.15 g horizontally and 0.10 g vertically.

2.3 Rebar Arrangements

The containment wall is reinforced with hoop, meridional and diagonal rebars. A typical rebar arrangement for the cylindrical wall is shown in Fig. 5. The hoop and meridional rebars are divided into two groups and each group is placed close to the wall surface. The diagonal rebars are only in one group, which is placed close to the outer surface.

The details of the rebar arrangements for the cylindrical portion of the containment are described below. Each group of the hoop reinforcement consists of two layers of No. 18 rebars with 14 inch spacing and remains constant throughout the cylindrical portion of the containment. There are two kinds of the meridional rebars: primary and secondary. Each group of the primary meridional rebars contains one layer of No. 18 rebar with 12 inch spacing. The primary rebars remain constant in the cylindrical portion and extend into the dome of the containment. The secondary meridional rebars are placed at the bottom third of the cylinder, i.e., from the basemat to the elevation of 54'-10" (zero elevation at base is used in this report). The amount of secondary rebars is varied at different elevations as summarized in Table 1. It is noted that there is one out of six No. 18 secondary rebars continued from the bottom to the top. For simplicity, it is replaced by smaller size rebars in Table 1. In addition, some secondary bars are bent at the lower portion of the containment, these bends are neglected.

For the dome portion of the containment, each group of the hoop reinforcements consists of one layer of No. 14 rebars with 8 inch spacing for vertical angle from zero (spring line) to 55°. However, spacing of 8-1/4 inch is used near the outside face from zero to 9.5°. For vertical angle from 55° to 90° (top), one layer of No. 14 rebars with 9 inch spacing is used.

The meridional rebar arrangements in the dome portion is sketched in Fig. 6. The primary meridional reinforcement of the cylinder extends into the dome along the meridians. The distance between meridional bars along the parallel decreases as one moves up from the springline, and therefore, the quantity of

steel per unit length along the meridian increases above the design value. When this later steel quantity becomes twice the design value, i.e., at 60° from the springline, each pair of meridional bars are combined into one bar, by the help of appropriate transition splices. The reinforcement quantity is halved again at 75° , 83° and 86° from the springline. Thus, the quantity of meridional steel per unit length along the parallel is kept between the design value and twice the design value, to avoid reinforcement congestion and waste of material. A summary of dome reinforcements is shown in Table 2.

A layer of diagonal rebars at $+45^\circ$ and -45° with the vertical is placed near the outer surface to take the in-plane seismic shear forces as shown in Fig. 5. These seismic diagonal bars extend into the bottom third of the dome. The amount of reinforcing is varied at different elevations and is shown in Tables 1 and 2.

3.0 CONTAINMENT MODELLING

In order to utilize the finite element analysis results in computing the limit state probabilities, the containment modelling should be made in such a way that the local coordinates of the elements have the same directions as those of the rebars. This is very easy to achieve in this study, since all the rebars are in the hoop and meridional directions.

The finite element utilized in the analysis is the shell element as described in the SAPV computer code. A three-dimensional finite element model as shown in Fig. 7 is used for the structural analysis of the containment. The side and top views of the containment are shown in Figs. 8 and 9, respectively. Also, a detailed cross-sectional view of the containment is shown in Fig. 10. As can be seen from this figure, the containment is divided into 23 layers. Except at the top of the dome, each layer has 24 elements such that the nodal points are taken every 15° in the circumferential direction. This discretization requires a total of 553 nodes and 540 elements.

The boundaries of the elements are made such that it matches the change of the reinforcements. Hence, the amount of reinforcements in most of the elements is the same as shown in Tables 1 and 2. However, the meridional rebars in the dome portion are varied in different elevations, an average value of the meridional reinforcement in these elements is used. It is noted that the diagonal rebars, which provide in-plane seismic shear resistance, are not included in the present analysis.

A welded steel liner with a minimum thickness of 1/4-inch is attached to the inside face of the concrete shell to insure a high degree of leak-tightness. The liner is disregarded as a load carrying structural component in the analysis. Furthermore, such other complications as penetrations, personnel lock and equipment hatches are not included in the study.

4.0 MATERIAL PROPERTIES

In order to perform a reliability analysis on a containment structure, it is necessary to determine the actual material properties. In the present study, the mean values of the material properties are used in the analysis. The variation of material properties will be included in the sensitivity studies in the future. The properties for the concrete and rebars are summarized as follows:

A) Concrete

The minimum compressive strength of concrete at 28 days used for the Indian Point Unit No. 3 containment is 3000 psi. The weight density of the concrete is taken to be 150 lb/ft³. Young's modulus and Poisson's ratio are 3.1×10^6 psi and 0.2, respectively. For the 28 day compressive strength f_c , a statistical analysis of the available data was carried out at BNL to determine its statistical characteristics. The mean value and standard deviation are estimated to be 4896 psi and 627 psi, respectively.

B) Reinforcing Bars

As can be seen from Tables 1 and 2, No. 18 rebars are the main reinforcement used in the containment structure. Hence, the statistics for No. 18 rebars is used to represent all other types of rebars. Young's modulus and Poisson's ratio are taken to be 29.0×10^6 psi and 0.3, respectively. A statistical analysis was carried out for the No. 18 rebars, the mean and standard deviation of the yield strength f_y are estimated to be 71.8 and 5.18 ksi, respectively.

5. PROBABILISTIC MODELS FOR LOADS

Various static and dynamic loads act on the containment structure during its lifetime. These loads may be caused by normal operating, environmental and accidental conditions. Since the loads intrinsically involve random and other uncertainties, an appropriate probabilistic model for each load must be established.

5.1 Dead Load

As mentioned in Section 2.2, the dead load primarily arises from the weights of the containment wall. It is noted that there are some uncertainties as to the actual magnitude of the dead load.⁸ For the purpose of this analysis, however, dead load is assumed to be deterministic and is equal to the design value, which is computed based on the weight density of reinforced concrete as 150 lb/ft³.

5.2 Accidental Pressure

The accidental pressure is considered as a quasi-static load and it is uniformly distributed on the containment wall. The accidental pressure is idealized as a rectangular pulse and will occur in accordance with the Poisson law during the containment life. Under these assumptions, three parameters are required to model the internal pressure: the occurrence rate λ_p (per year), the mean duration μ_{dp} (in seconds) and the intensity P .

For the Indian Point Unit No. 3 containment, the mean duration is taken to be 1200 seconds. This value is obtained from the approximation of the time history shown in Fig. 4. According to the Indian Point Probabilistic Safety Study⁹, the mean occurrence rate for a large LOCA is $2.16 \times 10^{-3}/\text{yr}$, which is used in the analysis.

The intensity of the accidental pressure is treated as a Gaussian random variable. Unfortunately, there is no actual data to determine its statistics, i.e., the mean value and the standard deviation. Nevertheless, the consensus survey of the nuclear structural loads, which was carried out by BNL, indicates that the ratio of the mean value to the design value is 0.89 and the coefficient of variation is 0.12.¹⁰ Since the design value of the accidental pressure for the Indian Point Unit No. 3 containment is 47 psi, the mean value, \bar{P} , and the standard deviation, σ_p , are computed as follows:

$$\begin{aligned}\bar{P} &= 47 \times 0.89 = 41.83 \text{ psi} \\ \sigma_p &= 0.12 \times 41.83 = 5.02 \text{ psi}\end{aligned}$$

5.3 Earthquake Ground Acceleration

The earthquake ground acceleration is assumed to act only along the global x direction. It is further assumed that the ground acceleration can be idealized as a segment of finite duration of a stationary Gaussian process with mean zero and a Kanai-Tajimi spectrum. The Kanai-Tajimi spectrum has the following expression:

$$S_{ggxx}(\omega) = S_0 \frac{1 + 4\zeta_g^2(\omega/\omega_g)^2}{[1 - (\omega/\omega_g)^2]^2 + 4\zeta_g^2(\omega/\omega_g)^2} \quad (1)$$

where the parameter S_0 represents the intensity of the earthquake and ω_g and ζ_g are the dominant ground frequency and the critical damping, respectively. The values of ω_g and ζ_g depend on the soil conditions of the containment site. For the Indian Point Unit No. 3 Power Plant, the soil condition is determined as rock.⁷ For such a soil condition, Reference 11 recommends that the values of ω_g and ζ_g in Eq. 1 are equal to 8π rad/sec and

0.6, respectively. The mean duration μ_{dE} of the earthquake acceleration is assumed to be 15 seconds in this study. The peak ground acceleration A_1 , given an earthquake, is assumed to be $A_1 = p_g \alpha_g$ where p_g is the peak factor which is assumed to be 3.0 in this study. The standard deviation of the ground acceleration, α_g , is computed by integrating the Kanai-Tajimi spectral density function with respect to ω . Explicitly written, the standard deviation α_g is

$$\alpha_g = \sqrt{\pi \omega_g \left(\frac{1}{2\zeta_g} + 2\zeta_g \right)} \sqrt{S_0} \quad (2)$$

The peak ground acceleration A_1 , given an earthquake, can be rewritten as

$$A_1 = \alpha_g \sqrt{S_0}, \quad (3)$$

where

$$\alpha_g = p_g \sqrt{\pi \omega_g \left(\frac{1}{2\zeta_g} + 2\zeta_g \right)} \quad (4)$$

If the earthquake occurs in accordance with the Poisson law at a rate λ_E per year, it is easy to show that the probability distribution $F_A(a)$ of the annual peak ground acceleration A is related to the probability distribution $F_{A_1}(a)$ of A_1 in the following fashion.

$$F_A(a) = \exp \{-\lambda_E [1 - F_{A_1}(a)]\}$$

or

(5)

$$F_{A_1}(a) = 1 + \frac{1}{\lambda_E} \ln F_A(a)$$

Therefore, if a_0 indicates the minimum peak ground acceleration for any ground shaking to be considered an earthquake, $F_{A_1}(a_0) = 0$ and hence, $\lambda_E = -\ln F_A(a_0)$. Assuming that $F_A(a)$ is of the extreme distribution of Type II, i.e.,

$$F_A(a) = \exp[-(a/\mu)^{-\alpha}] \quad (6)$$

where α and μ are two parameters to be determined. By least square fitting to the hazard curve given in the PRA study⁹, we find $\alpha = 3.14$ and $\mu = 0.0135$.

From Eqs. 5 and 6, we obtain:

$$F_{A_1}(a) = 1 - (a/a_0)^{-\alpha} \quad a \geq a_0 \quad (7)$$

Under these conditions, one finds that $\lambda_E = 1.64 \times 10^{-2}/\text{year}$ for $a_0 = 0.05$ g. Combining Eqs. 3 and 7, and writing Z for $\sqrt{S_0}$, we further obtain the probability distribution and density functions of Z in the forms, respectively,

$$\left. \begin{aligned} F_Z(z) &= 1 - (\alpha_g z/a_0)^{-\alpha} \\ f_Z(z) &= \alpha(\alpha_g/a_0)(\alpha_g z/a_0)^{-(\alpha+1)} \end{aligned} \right\} \quad \text{for } z \geq a_0/\alpha_g \quad (8)$$

The information about the maximum earthquake ground acceleration, a_{\max} , which represents the largest earthquake possible to occur at a particular site, is needed in order to determine the limit state probability. In this study, a_{\max} is chosen to be equal to 0.71 g.

The parameters of the loading conditions described in this section are summarized in Table 3.

6. FINITE ELEMENT ANALYSIS OF THE CONTAINMENT

When a reinforced concrete containment is subjected to static and dynamic loads, its cross-section will usually produce cracks, the extent of which depends on the load history. Because of the complexity of the various load combinations, however, it is difficult to predict a priori the crack patterns for all conceivable combinations of loadings. While a linear elastic analysis cannot take into account the temporal variations of the structural stiffness which result from such a dependence on load history, it will nevertheless, in most instances yield approximately correct stress resultants for the various

sections of the structure. This is especially the case if the section material properties are adjusted to reflect the concrete cracking. To account the cracking effect, the stiffness of the element is taken to be one half of that of the uncracked section in this study.

6.1 Static Analysis

As mentioned in Section 5, dead load and accidental pressure are considered to be static loads acting on the containment. Using the finite element model described in Section 3, a static analysis of the containment due to dead load alone was performed, and results are shown in Table 4. Similarly, the analysis of the containment due to unit accidental pressure alone is also carried out and the results are shown in Table 5. These results are going to be used in the reliability analysis.

6.2 Dynamic Analysis

For dynamic analysis of structures, modal analysis is employed. Hence, the dynamic characteristics of the structures are represented by the natural frequencies and associated mode shapes. Using the model described in Section 3, the first twenty (20) natural frequencies are evaluated and are shown in Table 6. The mode shapes for the first and second pairs of bending modes (modes 1, 2, 15, 16) are shown in Figs. 11 and 12. It is important to choose the significantly participating modes for the reliability analysis. In this study, only the first and second pairs of bending modes are included in the analysis.

7. LIMIT STATE FOR THE CONTAINMENT

For the reinforced concrete containment, if an onset of the structural failure is of interest, the limit state may be defined as follows. The structural response is considered to have reached the limit state if the rebars begin to yield (in tension or compression) and/or if the crushing strength of the concrete is reached at the cross-section's extreme fiber during the service life of the containment.

The analytical expressions for the limit state introduced previously are as follows:

$$f_s \geq f_y \quad (9)$$

$$f_c \geq 0.85 f'_c \quad (10)$$

where f_s is the stress in the rebars and f_y is the steel yield strength, f_c is the compressive concrete stress at the extreme fibers and f'_c is the concrete compressive strength.

Based on, (a) the above definition of the limit state, (b) the assumption of a linear stress-strain relationship, and (c) the conventional theory of reinforced concrete, which asserts that concrete cannot take any tension, the limit state surface in terms of the membrane stress τ and bending moment m /unit length can be established for a specific cross-section at the finite element boundaries.¹² A typical limit state surface for a element is shown in Fig. 13, and the coordinates are listed in Table 7. Point 'a' represent a limit state under pure (uniform) compression and point 'g' a limit state under pure (uniform) tension. In the same figure, lines I (\overline{ac} and $\overline{ac'}$), lines II (approximated by \overline{ce} and $\overline{c'e'}$), lines III (\overline{ef} and $\overline{e'f'}$) and lines IV (\overline{fg} and $\overline{f'g'}$) indicate those parts of the limit state surface in which the limit states are reached in concrete crushing with cross-sections remaining uncracked (lines I), in concrete crushing with partially cracked cross-sections (lines II), in yielding of rebars in tension with partially cracked cross-sections (lines III) and in yielding of rebars in tension with totally cracked cross-sections (lines IV).

8. RELIABILITY ANALYSIS RESULTS

The reliability analysis methodology used in this study is summarized in Ref. 3. Based on this reliability analysis method, the structural model, loading conditions and the limit state described in the preceding section, the reliability analysis for the Indian Point Unit No. 3 containment structure was made. The results are presented in this section.

8.1 Dead Load and Accidental Pressure (D+P)

The load characteristics of the dead load and the accidental pressure due to a large LOCA are described in Sections 5.1 and 5.2, respectively. A reliability analysis is carried out to estimate the probability that the limit state will be reached under the simultaneous action of this accidental pressure and the dead load during the forty year lifetime of the containment.

The conditional limit state probability for each element is tabulated in Table 8 and plotted in Fig. 14. From the table, it can be seen that the critical elements are the elements denoted as 289 to 312, which are located in the first layer of the dome section just above the spring line. Since the structure and the loads are both axisymmetrical in this case, all the elements located at the same level have the same limit state probability. The limit state is reached as the hoop rebars in the critical elements begin to yield. When these conditional probabilities are multiplied by the expected number $T\lambda_p = 8.64 \times 10^{-2}$ of such simultaneous occurrences during the containment life of forty years, the unconditional limit state probabilities $P_f^{(D+P)}$ under the simultaneous action of D and P is obtained, and is equal to 6.79×10^{-6} .

8.2 Dead Load and Earthquake Ground Acceleration (D+E)

An idealization of the earthquake ground acceleration is presented in Section 5.3. For the combination of the dead load and earthquake ground acceleration, the conditional limit state probability $P^{(D+E)}$ for the containment are shown in Table 9 and plotted in Fig. 14. From the table, it can be seen that the critical elements are elements 6, 7, 18 and 19. These elements are located in the lowest finite element layer and immediately adjacent to the global x axis. In this case, the limit state is reached as the meridional reinforcing bars in the critical elements begin to yield. The locations of the critical elements and the manner in which the limit state is reached are obviously consistent with the structural and loading symmetry with respect to the x-axis under this particular load combination. The lower and upper bounds of the conditional limit state probability $P^{(D+E)}$ are found to be 0.92×10^{-7} and

1.64×10^{-7} , respectively. Multiplying these bounds by the expected number $T\lambda_E = 6.56 \times 10^{-1}$ of simultaneous occurrences of D and E, the lower and upper bounds of the unconditional limit state probability $P_f^{(D+E)}$ under this load combination during the containment life of forty years are obtained as 0.60×10^{-7} and 1.07×10^{-7} , respectively. Since these two bounds are in a relatively narrow range within the same order of magnitude, any value between these two bounds may be used as a reasonable approximation for the limit state probability.

8.3 Dead Load, Earthquake Ground Acceleration and Accidental Pressure (D+E+P)

The probabilistic characteristics of the loads indicated in the sub-section title above are described in Section 5. Under the combination of these loads, the conditional limit state probability are listed in Table 10 and also plotted in Fig. 14. The critical elements are found to be elements 294, 295, 306 and 307, which are located immediately adjacent to the global x-axis (when projected onto a horizontal plane) at the first layer above the springline. This is the same level at which the critical elements are found under the D+P load combination (Section 8.1). The manner in which the limit state is reached is also the same as for the D+P combination (i.e., yielding of the hoop rebars). The lower and upper bounds of the conditional limit state probability $P^{(D+E+P)}$ under this load combination are 4.89×10^{-4} and 5.80×10^{-4} , respectively. Multiplying these bounds by $T\lambda_{D+E+P} = 5.46 \times 10^{-8}$ provides the lower and upper bounds of the unconditional probability under this load combination during the containment life of forty years; the lower bound = 2.67×10^{-11} and the upper bound = 3.17×10^{-11} .

Comparing the limit state probabilities under the load combination D+P with those under the combination D+E+P, it is observed that (1) the mode in which the limit state is reached (yielding of the hoop rebars) in the critical elements is the same and (2) the critical elements under the current load combination D+E+P comprise the four elements which are most stressed by the additional earthquake load among those critical elements under the load combination D+P. These observations suggest that the accidental pressure P is a

dominant factor in controlling the conditional limit state probability. The substantial reduction in the values of the lower and upper bounds of the unconditional probability $P_f^{(D+E+P)}$, as compared with $P_f^{(D+P)}$, is primarily attributable to the fact that $T\lambda_{D+E+P} = 5.46 \times 10^{-8}$ is much smaller than $T\lambda_{D+P} = 8.64 \times 10^{-2}$.

8.4 Overall Limit State Probability

The limit state probabilities evaluated in the preceding section are those at the critical elements within the containment under various load combinations. While the limit state probability of the containment as a whole, or the system limit state probability, under a certain load combination is always larger than that of the critical elements, the author's experience in structural reliability analysis suggests that the difference between the system limit state probability and the limit state probability of the critical elements is tolerable for the type of load-structure system under consideration. Therefore, for the sake of analytical simplicity and computational economy, the present study approximates the containment limit state probability under each load combination by the critical element limit state probability as evaluated in Sections 8.1 to 8.3. The limit state probabilities, conditional and unconditional, under various load combinations are summarized in Table 11. Under the assumption that the containment will not fail under dead load alone, the overall containment limit state probability P_f is then obtained as the sum of the limit state probabilities under all these (mutually exclusive) load combinations. Hence, the containment limit state probability is 6.85×10^{-6} - 6.90×10^{-6} for its lifetime of forty years.

9. RESULTS FOR DIFFERENT LIMIT STATE

The results presented in the previous section (i.e., Section 8) are corresponding to the onset of the structure failure. If more substantial failure of structures is of interest, the limit state representing this condition can be defined based on the reinforced concrete ultimate strength theory. Essentially, the limit state is reached when a maximum compressive strain at the extreme fiber of the cross-section is equal to 0.003, while the yielding of rebars is permitted. Under this definition of the limit state, a limit state

surface for each element may be constructed. Utilizing this limit state surface, the reliability analysis of Indian Point Unit 3 containment under the loading described in Section 5, is also carried out. The results are summarized in Table 12. For most load combinations, the limit state probabilities in Table 12 is about one order of magnitude less than those shown in Table 11, while the critical elements remain the same.

10. CONCLUDING REMARKS

The reliability analysis method developed by BNL is applied to the Indian Point Unit No. 3 containment structure under dead load, accidental pressure and earthquake ground acceleration. The results are presented in this report. This is the first attempt to carry out the reliability analysis for the existing containment structures in order to evaluate the reliability levels implied in the design criteria. It is noted that the estimated reliability levels are affected by the judgements made in the design process and the assumptions made in the reliability evaluation. In order to reasonably assess the reliability levels implied in the design criteria, it is necessary to continue the efforts by carrying out the reliability analysis for other existing containment structures designed according to these criteria.

REFERENCES

1. ACI-ASME Joint Technical Committee, "Code for Concrete Reactor Vessels and Containments, ASME Boiler and Pressure Vessel Code Section III - Division 2", 1980.
2. USNRC, Standard Review Plan, Section 3.8.1, NUREG-0800, Rev. 1, 1981.
3. Hwang, H., Shinozuka, M., Brown, P. and Reich, M., "Reliability Assessment of Reinforced Concrete Containment Structures", BNL-NUREG-51661, NUREG/CR-3227, February, 1983.
4. Kako, T., Shinozuka, M., Hwang, H. and Reich, M., "FEM-Based Random Vibration Analysis of Nuclear Structures Under Seismic Loading", SMIRT-7 Conference Paper K 7/2, Chicago, IL, August 22-26, 1983.
5. Shinozuka, M., Kako, T., Hwang, H. and Reich, M., "Development of a Reliability Analysis Method for Category I Structures", SMIRT-7 Conference Paper M 5/3, Chicago, IL, August 22-26, 1983.
6. Shinozuka, M., Kako, T., Hwang, H., Brown, P. and Reich, M., "Estimation of Structural Reliability Under Combined Loads", SMIRT-7 Conference Paper M 2/3, Chicago, IL, August 22-26, 1983.
7. Power Authority of the State of New York, "Indian Point Nuclear Power Plant, Unit 3, Final Safety Analysis Report", Docket 50286.
8. Hwang, H., Wang, P.C. and Reich, M., "Probabilistic Models for Operational and Accidental Loads on Seismic Category I Structures", BNL-NUREG-51682, NUREG/CR-3342, June 1983.
9. Power Authority of the State of New York, "Indian Point Probabilistic Safety Study", Docket 50247, March 1982.

REFERENCES (Cont'd)

10. Hwang, H., Wang, P.C., Shooman, M. and Reich, M., "A Consensus Estimation Study of Nuclear Power Plant Structural Loads", BNL-NUREG-51678, NUREG/CR-3315, May 1983.
11. Ellingwood, B., Batts, M.E., "Characterization of Earthquake Forces for Probability-Based Design of Nuclear Structures", BNL-NUREG-51587, NUREG/CR-2945, Sept. 1982.
12. Chang, M., Brown, P., Kako, T., Hwang, H., "Structural Modeling and Limit State Identification for Reliability Analysis of RC Containment Structures", SMIRT-7 Conference Paper M 3/2, August 22-26, 1983.

Table 1 Cylinder Reinforcement.

Elevation	Hoop	Meridional		Diagonal
		Primary	Secondary	
0 to 25'-0"	2#18 @ 14in	1#18 @ 12in	1#18 @ 12in	1#18 @ 30in
25'-0" to 45'-5"	"	"	1#11 @ 12in	"
45'-5" to 50'-3"	"	"	2#11 @ 36in	"
50'-3" to 54'-10"	"	"	1#11 @ 36in	"
54'-10" to 110'-6"	"	"		"
110'-6" to 148'-0"	"	"		1#18 @ 60in + 1#14 @ 60in

Table 2 Dome Reinforcement.

Angle From Spring-Line (Degrees)	Hoop	Meridional	Diagonal
0°-9.5°	1#14 { @ 8-1/4" outside @ 8.0" inside	1# 18 @ 0.796°	1#18+1#14 @ 4° (horiz. dist.)
9.5°-18.5°	1#14 @ 8.0 in	"	"
18.5°-35°	"	"	1#11 @ 2° (horz. dist.)
35°-55°	"	"	"
55°-60°	1#14 @ 9.0 in	"	"
60°-75°	"	1#18 @ 1.593°	"
75°-83°	"	1#18 @ 3.136°	"
83°-86°	"	1#18 @ 6.37°	"
86°-90°	"	1#18 @ 12.74°	"

Table 3 Load Parameters.

Load	Load Parameters
Dead Load (D)	*Deterministic and time invariant
Accidental Pressure due to a LOCA (P)	*Occurrence rate $\lambda_P = 2.16 \times 10^{-3}/\text{year}$ *Mean duration $\mu_{dP} = 1200$ seconds *P = Gaussian with mean value $\bar{P} = 41.83$ psi and standard deviation $\sigma_P = 5.02$ psi
Earthquake Load (E)	*Stationary random process (a segment of 15 seconds) with a Kanai-Tajimi spectrum

$$S_{gg}(\omega) = S_0 \frac{1 + 4\zeta_g^2(\omega/\omega_g)^2}{[1 - (\omega/\omega_g)^2]^2 + 4\zeta_g^2(\omega/\omega_g)^2}$$

where $\omega_g = 8\pi$ rad/sec and $\zeta_g = 0.6$

*Distribution function of $Z = \sqrt{S_0}$

$$F_Z(z) = 1 - (\alpha_g z / a_0)^{-\alpha}$$

where

$$\alpha_g = P_g \sqrt{\pi \omega_g [1/(2\zeta_g) + 2\zeta_g]}$$

with $P_g = 3.0$, $a_0 = 0.05g$ and $\alpha = 3.14$;
 $a_{\max} = 0.71g$

*Occurrence rate $\lambda_E = 1.64 \times 10^{-2}/\text{year}$

*Mean duration $\mu_{dE} = 15$ seconds

Table 4 Stresses Due to Dead Load.

Element Number	Local X-Direction		Local Y-Direction	
	Axial Stress S_{xx} (psi)	Moment M_{xx} (pound-in/in)	Axial Stress S_{yy} (psi)	Moment M_{yy} (pound-in/in)
529 - 540	- 35.4	- 0.144×10^4	- 35.3	- 0.163×10^4
505 - 528	- 34.8	- 0.144×10^4	- 35.6	- 0.132×10^4
481 - 504	- 33.4	- 0.137×10^4	- 35.8	- 0.134×10^4
457 - 480	- 30.7	- 0.132×10^4	- 36.4	- 0.131×10^4
433 - 456	- 26.4	- 0.126×10^4	- 37.4	- 0.129×10^4
409 - 432	- 19.0	- 0.123×10^4	- 39.2	- 0.141×10^4
385 - 408	- 4.09	- 0.112×10^4	- 42.6	- 0.135×10^4
361 - 384	17.7	- 0.252×10^3	- 49.2	0.120×10^4
337 - 360	30.5	0.614×10^3	- 57.6	0.356×10^4
313 - 336	31.9	0.107×10^4	- 56.5	0.531×10^4
289 - 312	27.9	0.150×10^4	- 61.6	0.724×10^4
265 - 288	23.4	0.649×10^3	- 59.2	0.324×10^4
241 - 264	14.7	- 0.678×10^3	- 66.0	- 0.339×10^4
217 - 240	5.67	- 0.102×10^4	- 75.4	- 0.510×10^4
193 - 216	0.53	- 0.465×10^3	- 88.4	- 0.232×10^4
169 - 192	- 0.65	- 0.139×10^2	- 111.8	- 0.694×10^2
145 - 168	0.19	- 0.683×10^2	- 140.5	- 0.341×10^3
121 - 144	1.55	0.378×10^2	- 158.7	0.189×10^3
97 - 120	- 1.07	0.826×10^3	- 174.3	0.413×10^4
73 - 96	- 11.2	0.133×10^4	- 189.9	0.664×10^4
49 - 72	- 22.9	0.656×10^3	- 197.8	0.328×10^4
25 - 48	- 32.4	- 0.114×10^4	- 203.0	- 0.568×10^4
1 - 24	- 39.6	- 0.450×10^4	- 208.2	- 0.225×10^5

NOTE: 1. Local X direction is the same as hoop direction.
 2. Local Y direction is the same as meridional direction.

Table 5 Stresses Due to Unit Pressure.

Element Number	Local X-Direction		Local Y-Direction	
	Axial Stress S_{xx} (psi)	Moment M_{xx} (pound-in/in)	Axial Stress S_{yy} (psi)	Moment M_{yy} (pound-in/in)
529 - 540	9.74	0.201×10^1	9.73	0.540×10^2
505 - 528	9.72	0.574×10^1	9.73	0.262×10^2
481 - 504	9.72	$- 0.560 \times 10^1$	9.72	$- 0.112 \times 10^2$
457 - 480	9.74	$- 0.538 \times 10^1$	9.72	$- 0.472 \times 10^1$
433 - 456	9.75	$- 0.272 \times 10^1$	9.72	$- 0.236 \times 10^1$
409 - 432	9.76	0.241×10^1	9.72	0.138×10^2
385 - 408	9.72	0.172×10^1	9.69	0.550
361 - 384	9.91	$- 0.277 \times 10^2$	9.68	$- 0.111 \times 10^3$
337 - 360	10.6	$- 0.320 \times 10^2$	9.78	$- 0.111 \times 10^3$
313 - 336	11.0	$- 0.712 \times 10^2$	8.61	$- 0.291 \times 10^3$
289 - 312	11.8	$- 0.139 \times 10^3$	8.65	$- 0.642 \times 10^3$
265 - 288	12.4	$- 0.439 \times 10^2$	7.68	$- 0.219 \times 10^3$
241 - 264	13.7	0.106×10^3	7.68	0.529×10^3
217 - 240	14.8	0.134×10^3	7.68	0.670×10^3
193 - 216	15.4	0.651×10^2	7.68	0.320×10^3
169 - 192	15.4	$- 0.150 \times 10^1$	7.68	$- 0.748 \times 10^1$
145 - 168	15.5	$- 0.258 \times 10^2$	7.68	$- 0.129 \times 10^3$
121 - 144	15.9	0.156×10^2	7.68	0.781×10^2
97 - 120	15.0	0.277×10^3	7.68	0.138×10^4
73 - 96	11.5	0.439×10^3	7.68	0.219×10^4
49 - 72	7.61	0.179×10^3	7.68	0.897×10^3
25 - 48	4.50	$- 0.454 \times 10^3$	7.68	$- 0.227 \times 10^4$
1 - 24	2.26	$- 0.162 \times 10^4$	7.68	$- 0.809 \times 10^4$

Table 6 Natural Frequencies.

Mode Number	Frequencies (cycles/sec)
1	2.869
2	2.869
3	4.186
4	4.186
5	4.587
6	4.587
7	5.501
8	5.501
9	6.001
10	8.028
11	8.028
12	8.115
13	8.115
14	8.147
15	8.215
16	8.215
17	8.389
18	8.389
19	9.310
20	9.310

- NOTE: 1) Based on $E = E_c/2$, E_c = uncracked concrete stiffness.
 2) 1st pair of bending modes: Mode 1 and Mode 2.
 3) 2nd pair of bending modes: Mode 15 and Mode 16.

Table 7 Coordinates of Limit State Surface
(Element 289 - 312, Local X-Direction).

Point	Coordinate	
	τ (psi)	m (lb-in/in)
a	$- 4.56 \times 10^3$	1.13×10^4
c	$- 2.28 \times 10^3$	8.84×10^5
c'	$- 2.17 \times 10^3$	$- 8.73 \times 10^5$
e	$- 2.21 \times 10^2$	8.47×10^5
e'	$- 2.10 \times 10^2$	$- 8.71 \times 10^5$
f	5.14×10^2	1.96×10^5
f'	5.29×10^2	$- 2.21 \times 10^5$
g	8.29×10^2	$- 2.36 \times 10^4$

NOTE: See Figure 13 for reference.

Table 8 Conditional Limit State Probability $p(D+P)$.

Element No.	Local Direction	$p(D+P)$	$\log_{10} p(D+P)$	Critical Elements
529 - 540 (531)	X	4.02×10^{-13}	- 12.4	
505 - 528 (510)	X	3.59×10^{-13}	- 12.4	
481 - 504 (426)	X	5.36×10^{-13}	- 12.3	
457 - 480 (462)	X	9.08×10^{-13}	- 12.0	
433 - 456 (432)	X	1.98×10^{-12}	- 11.7	
409 - 432 (414)	X	5.46×10^{-12}	- 11.3	
385 - 408 (390)	X	1.83×10^{-17}	- 16.7	
361 - 384 (316)	X	2.27×10^{-17}	- 16.6	
337 - 360 (342)	X	5.87×10^{-13}	- 12.2	
313 - 336 (318)	X	5.54×10^{-6}	- 5.16	
289 - 312 (294)	X	7.86×10^{-5}	- 4.10	289, 290...312
265 - 288 (270)	X	7.40×10^{-34}	- 33.1	
241 - 264 (246)	X	5.32×10^{-25}	- 24.3	
217 - 240 (222)	X	3.75×10^{-19}	- 18.5	
193 - 216 (198)	X	5.31×10^{-17}	- 16.3	
169 - 192 (174)	X	3.75×10^{-17}	- 16.4	
145 - 168 (150)	X	8.20×10^{-17}	- 16.1	
121 - 144 (126)	X	4.12×10^{-15}	- 14.4	
97 - 120 (102)	X	7.68×10^{-18}	- 17.1	
73 - 96 (78)	X	5.12×10^{-41}	- 40.3	
49 - 72 (54)	X	1.45×10^{-141}	- 100	
25 - 48 (30)	Y	3.97×10^{-193}	- 100	
1 - 24 (6)	Y	1.77×10^{-39}	- 38.8	

Table 9 Conditional Limit State Probability $p^{(D+E)}$.

Element No.	Local Direction	$p^{(D+E)}$	$\log_{10} p^{(D+E)}$	Critical Elements
529 - 540 (531)		0	- 100	
505 - 528 (510)		0	- 100	
481 - 504 (486)		0	- 100	
457 - 480 (462)		0	- 100	
433 - 456 (432)		0	- 100	
409 - 432 (414)		0	- 100	
385 - 408 (390)	X	2.88×10^{-76}	- 75.5	
361 - 384 (316)	X	9.89×10^{-23}	- 42.0	
337 - 360 (342)	X	8.39×10^{-34}	- 33.1	
313 - 336 (318)	X	1.48×10^{-27}	- 26.8	
289 - 312 (294)	X	2.55×10^{-32}	- 31.6	
265 - 288 (270)	Y	$(1.39 - 1.39) \times 10^{-77}$	- 76.9	
241 - 264 (246)	Y	$(3.82 - 3.83) \times 10^{-50}$	- 49.4	
217 - 240 (222)	Y	$(2.94 - 2.99) \times 10^{-35}$	- (34.5 - 34.5)	
193 - 216 (198)	Y	$(3.69 - 3.86) \times 10^{-15}$	- (24.4 - 24.4)	
169 - 192 (174)	Y	$(5.51 - 6.58) \times 10^{-15}$	- (14.3 - 14.2)	
145 - 168 (150)	Y	$(1.37 - 1.96) \times 10^{-9}$	- (8.86 - 8.71)	
121 - 144 (126)	Y	$(2.43 - 4.54) \times 10^{-9}$	- (8.46 - 8.34)	
97 - 120 (102)	Y	$(1.41 - 1.73) \times 10^{-9}$	- (8.85 - 8.76)	
73 - 96 (78)	Y	$(3.69 - 3.89) \times 10^{-12}$	- (11.4 - 11.4)	
49 - 72 (54)	Y	$(1.46 - 1.68) \times 10^{-10}$	- (9.84 - 9.76)	
25 - 48 (30)	Y	$(3.48 - 4.76) \times 10^{-9}$	- (8.46 - 8.32)	
1 - 24 (6)	Y	$(0.917 - 1.64) \times 10^{-7}$	- (7.04 - 6.79)	6, 7, 18, 19

Table 10 Conditional Limit State Probability $p(D+E+P)$.

Element No.	Local Direction	$p(D+E+P)$	$\log_{10} p(D+E+P)$	Critical Elements
529 - 540 (531)	X	$(4.23 - 4.65) \times 10^{-13}$	- 12.4	
505 - 528 (510)	X	$(4.97 - 5.44) \times 10^{-13}$	- 12.3	
481 - 504 (486)	X	$(0.992 - 1.09) \times 10^{-12}$	- 12.0	
457 - 480 (462)	X	$(2.72 - 3.00) \times 10^{-12}$	-11.6 - -11.6	
433 - 456 (432)	X	$(1.64 - 1.86) \times 10^{-11}$	-10.8 - -10.7	
409 - 432 (414)	X	$(3.21 - 3.81) \times 10^{-10}$	- 9.49 - -9.42	
385 - 408 (390)	X	$(0.863 - 1.01) \times 10^{-11}$	-11.1 - -11.0	
361 - 384 (316)	X	$(2.53 - 2.63) \times 10^{-9}$	- 8.60 - -8.58	
337 - 360 (342)	X	$(3.11 - 3.32) \times 10^{-7}$	- 6.51 - -6.48	
313 - 336 (318)	X	$(1.38 - 1.63) \times 10^{-4}$	- 3.86 - -3.79	
289 - 312 (294)	X	$(4.09 - 5.80) \times 10^{-4}$	- 3.31 - -3.24	294, 295, 306, 307
265 - 288 (270)	Y	$(9.85 - 9.93) \times 10^{-21}$	- 20.0	
241 - 264 (246)	Y	$(1.24 - 1.24) \times 10^{-14}$	- 13.9	
217 - 240 (222)	Y	$(7.34 - 8.55) \times 10^{-12}$	-11.1 - -11.1	
193 - 216 (198)	Y	$(3.72 - 4.47) \times 10^{-10}$	- 9.43 - -9.35	
169 - 192 (174)	Y	$(1.61 - 2.20) \times 10^{-7}$	- 6.79 - -6.66	
145 - 168 (150)	Y	$(1.25 - 2.00) \times 10^{-5}$	- 4.90 - -4.70	
121 - 144 (126)	Y	$(0.828 - 1.21) \times 10^{-5}$	- 5.08 - -4.92	
97 - 120 (102)	Y	$(5.44 - 7.48) \times 10^{-6}$	- 5.26 - -5.13	
73 - 96 (78)	Y	$(4.85 - 5.76) \times 10^{-8}$	- 7.31 - -7.24	
49 - 72 (54)	Y	$(1.41 - 1.75) \times 10^{-7}$	- 6.85 - -6.76	
25 - 48 (30)	Y	$(1.40 - 1.75) \times 10^{-7}$	- 6.85 - -6.76	
1 - 24 (6)	Y	$(0.852 - 1.08) \times 10^{-7}$	- 7.07 - -6.96	

Table 11 Lifetime Limit State Probabilities.
(Based on Linear Stress Distribution)

Load Combination	Expected Number of Occurrences	Conditional Limit State Probabilities	Unconditional Limit State Probabilities	Critical Element
D+P	8.64×10^{-2}	7.86×10^{-5}	6.79×10^{-6}	289,290,...,312
D+E	6.56×10^{-1}	$(0.92 - 1.64) \times 10^{-7}$	$(0.60 - 1.07) \times 10^{-7}$	6,7,18,19
D+E+P	5.46×10^{-8}	$(4.83 - 5.80) \times 10^{-4}$	$(2.67 - 3.17) \times 10^{-11}$	294,295,306,307
Overall	---	---	$(6.85 - 6.90) \times 10^{-6}$	

NOTE: Assuming the containment will not fail under dead load alone.

Table 12 Lifetime Limit State Probabilities.
(Based on Nonlinear Stress Distribution)

Load Combination	Expected Number of Occurrences	Conditional Limit State Probabilities	Unconditional Probabilities	Critical Element
D+F	8.64×10^{-2}	3.99×10^{-7}	3.46×10^{-8}	289,290,...,312
D+E	6.56×10^{-1}	1.02×10^{-8}	6.72×10^{-9}	6,7,18,19
D+E+P	5.46×10^{-8}	$(1.57 - 1.68) \times 10^{-5}$	$(8.55 - 9.14) \times 10^{-13}$	294,295,306,307
Overall	---	---	4.13×10^{-8}	---

NOTE: Assuming the containment will not fail under dead load alone.

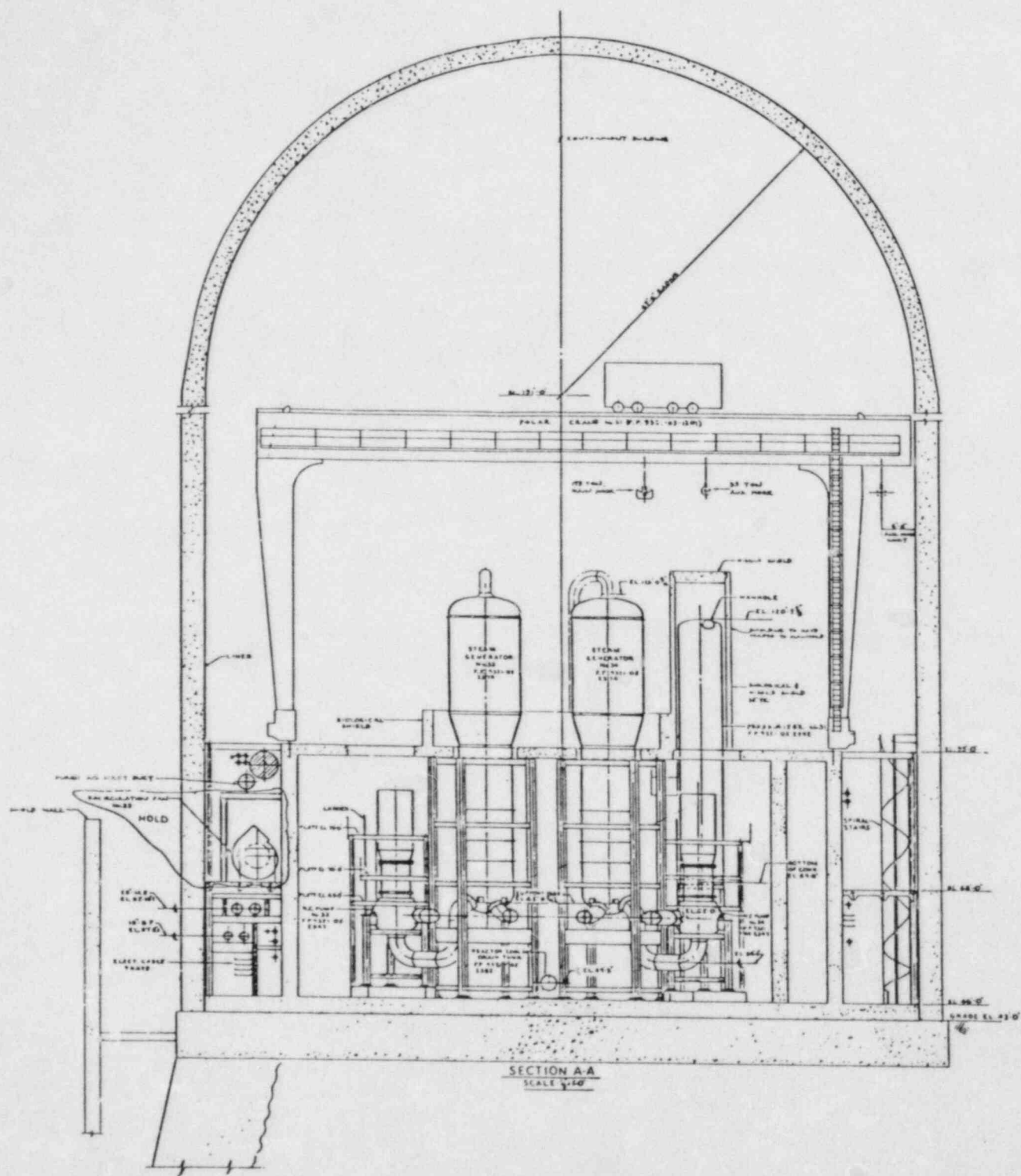


Fig. 1 Cross Section of Containment.
(Section A-A)

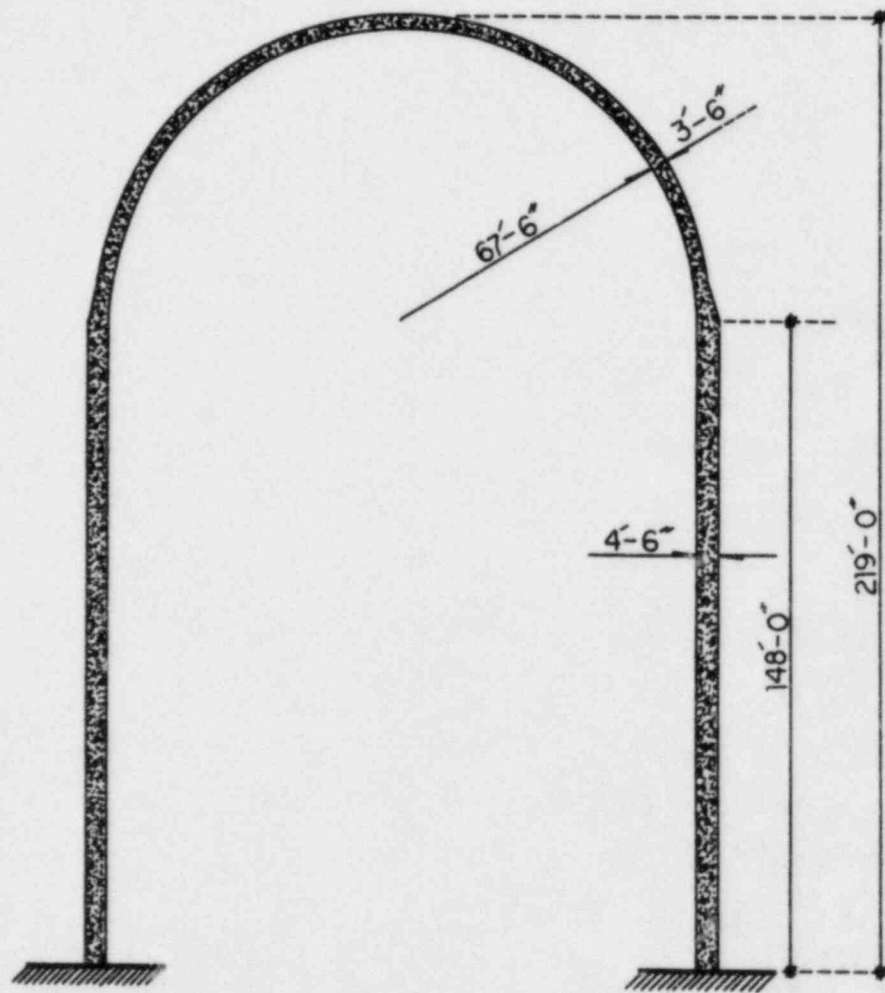


Fig. 3 Sketch of Containment Structure.

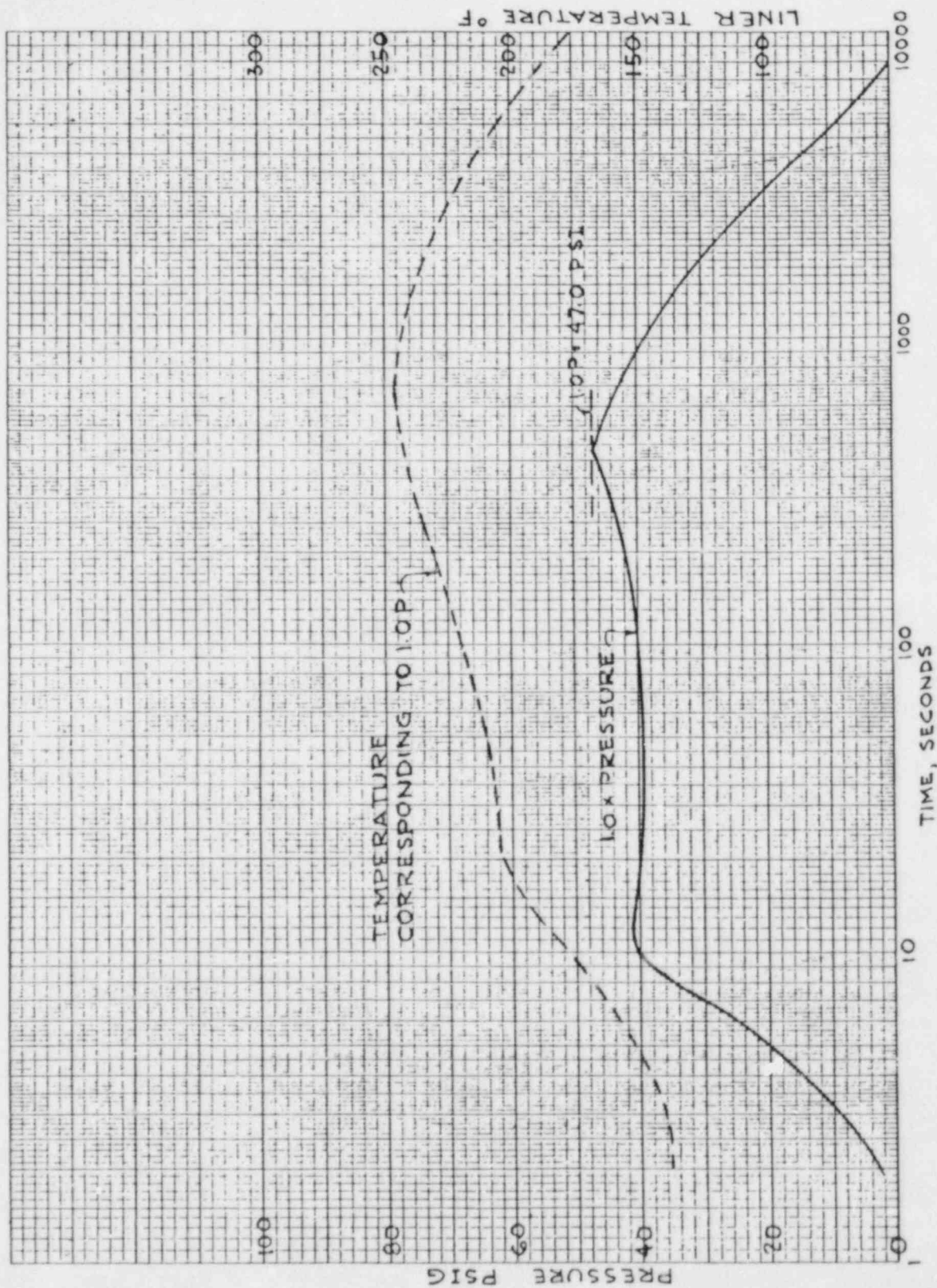


Fig. 4 Time Histories of Design Pressure and Temperature.

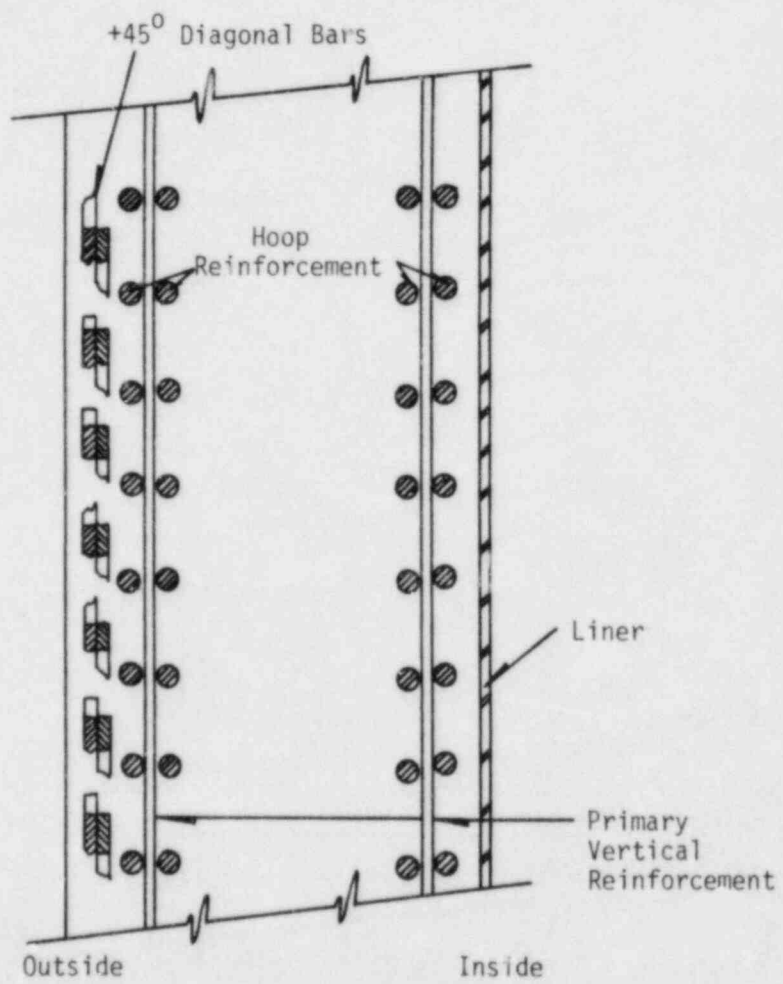


Fig. 5 Typical Rebar Arrangement for Cylindrical Wall.

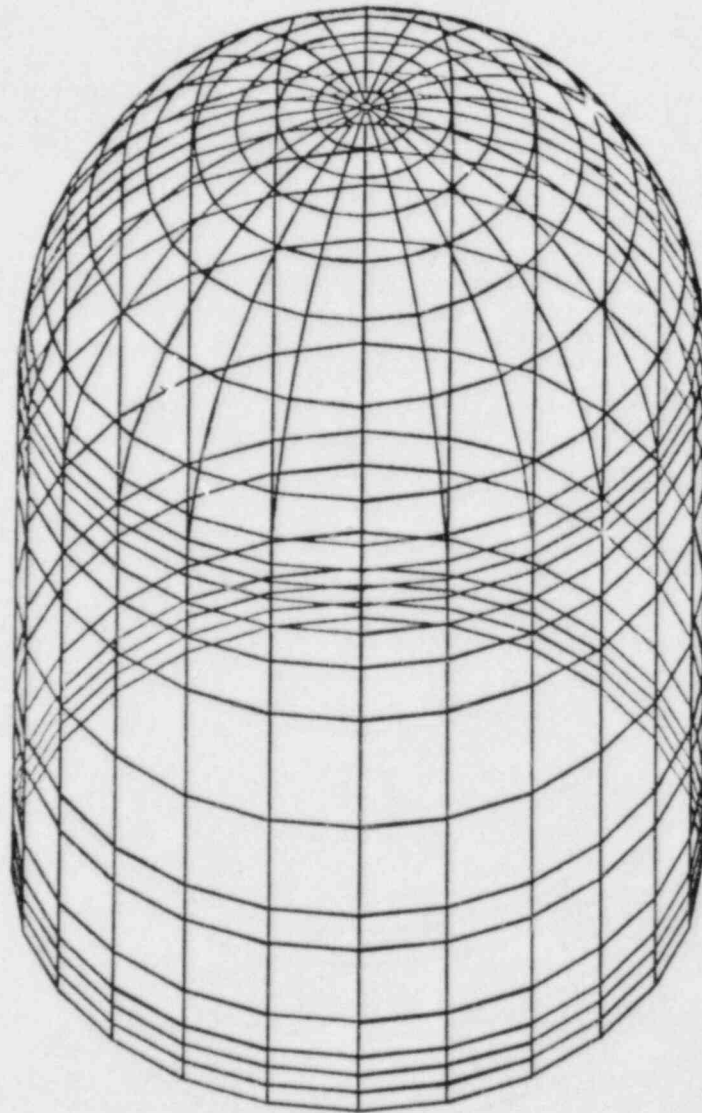


Fig. 7 Three-Dimensional Model for Containment.

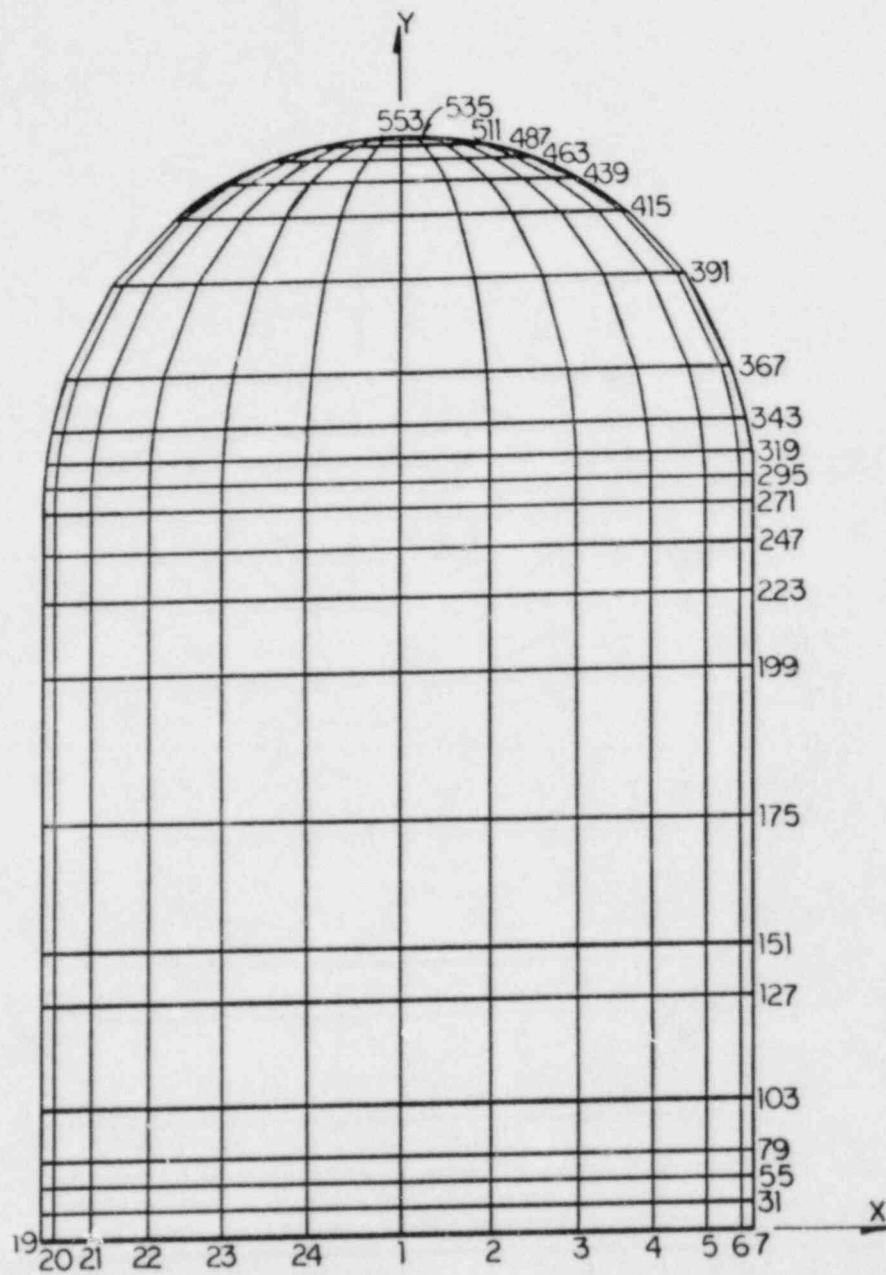


Fig. 8 Side View of Containment Model.

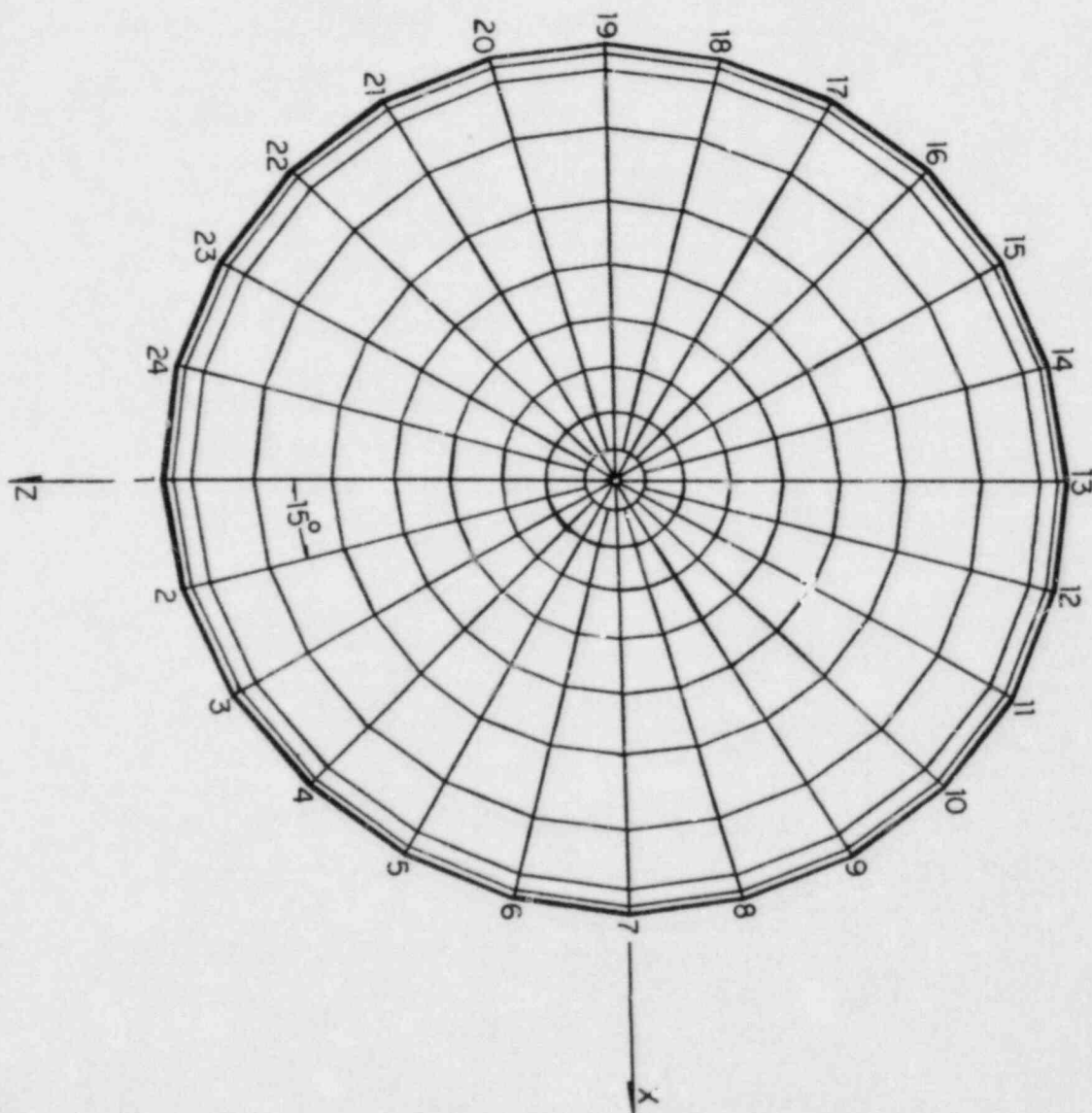


Fig. 9 Top View of Containment Model.

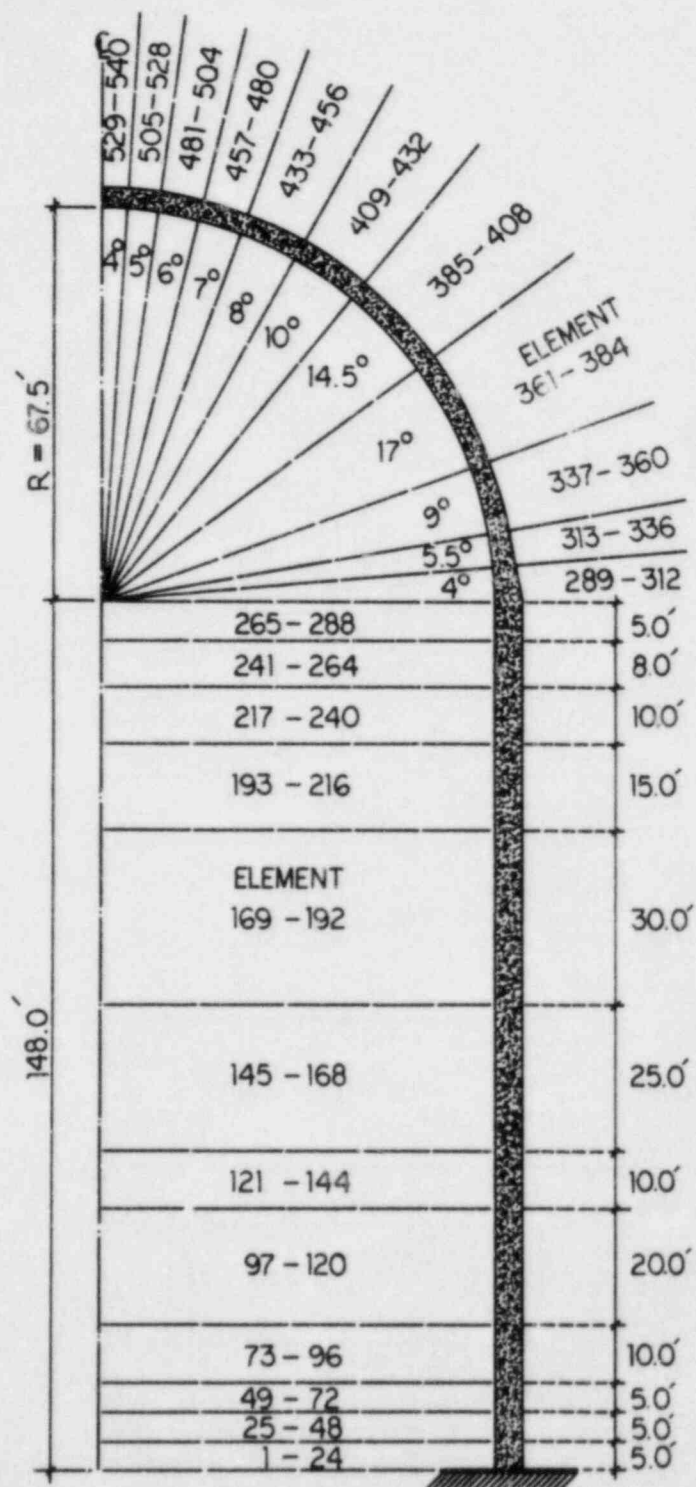


Fig. 10 Cross Section of Containment Model.

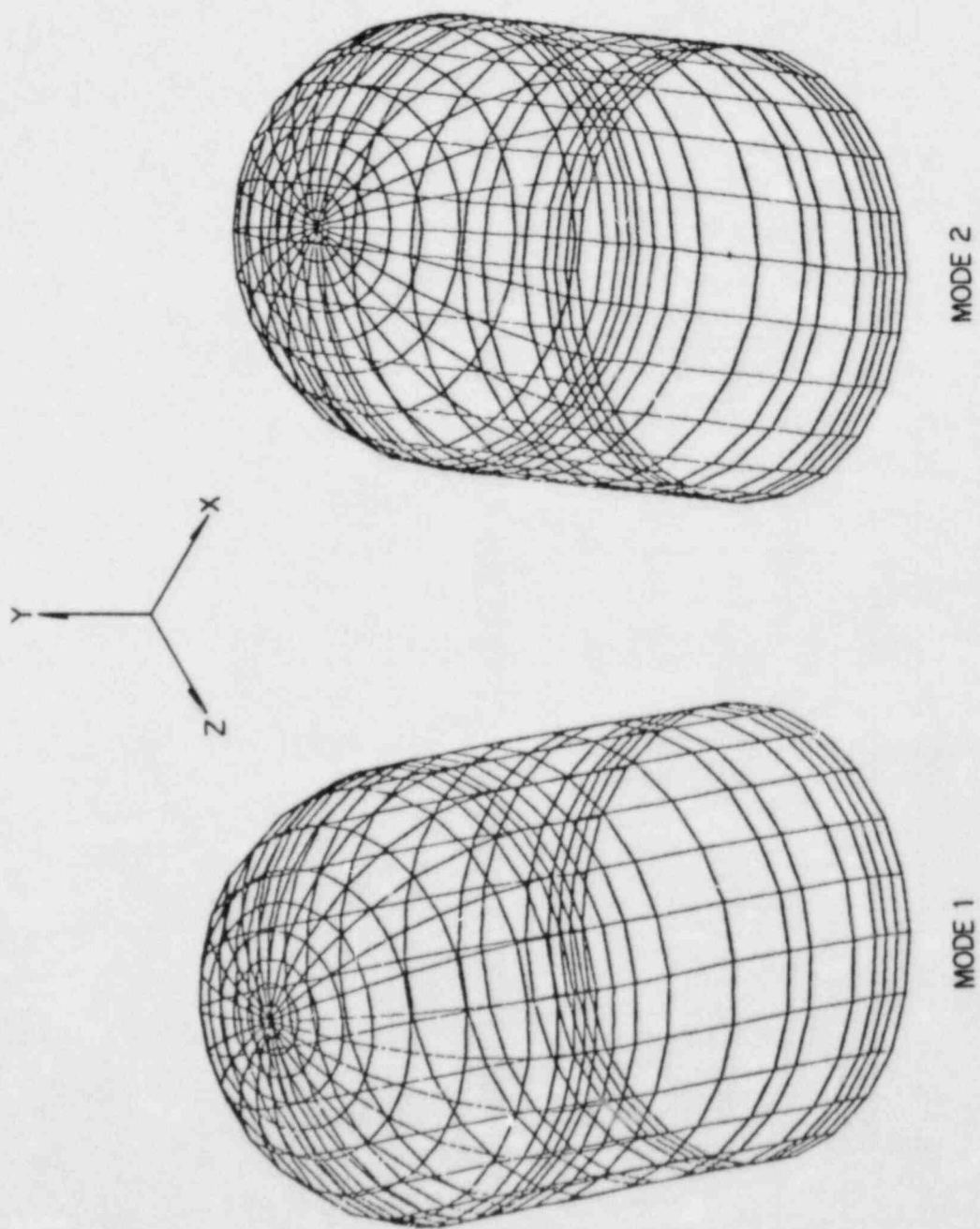


Fig. 11 Three-Dimensional Sketch of Mode Shapes (Modes 1 and 2).

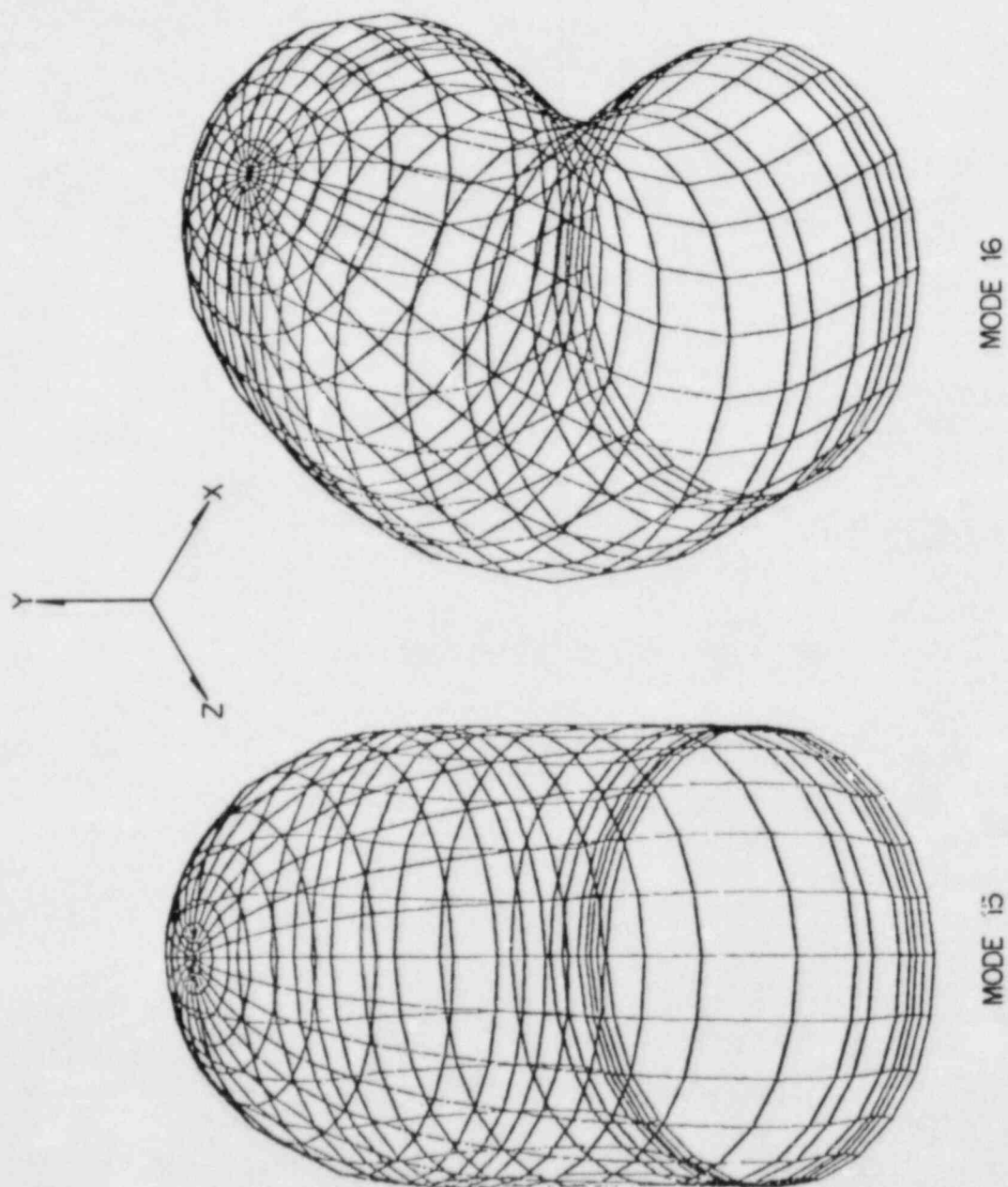


Fig. 12 Three-Dimensional Sketch of Mode Shapes (Modes 15 and 16).

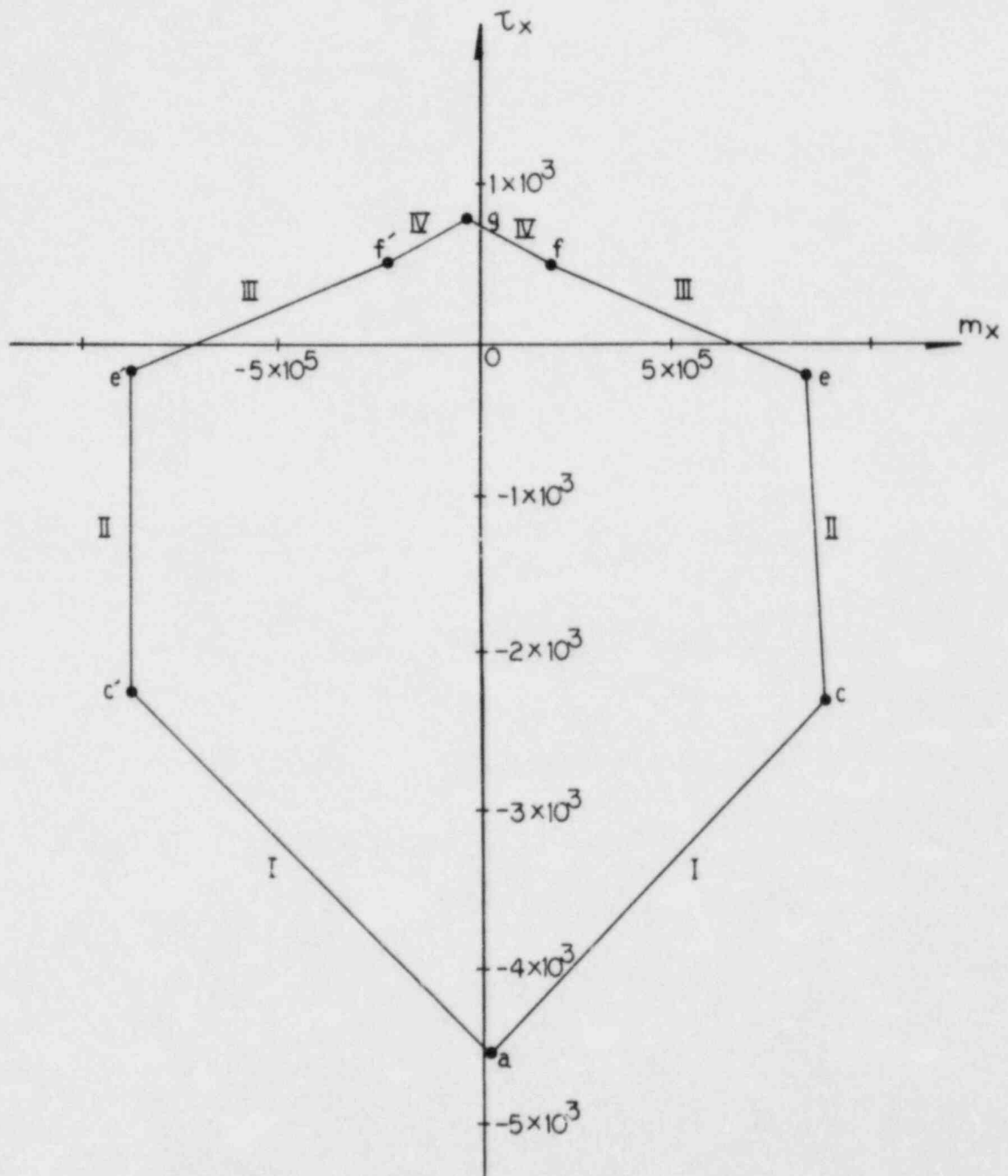


Fig. 13 Limit State Surface (Elements 289 - 312, Local X-Direction).

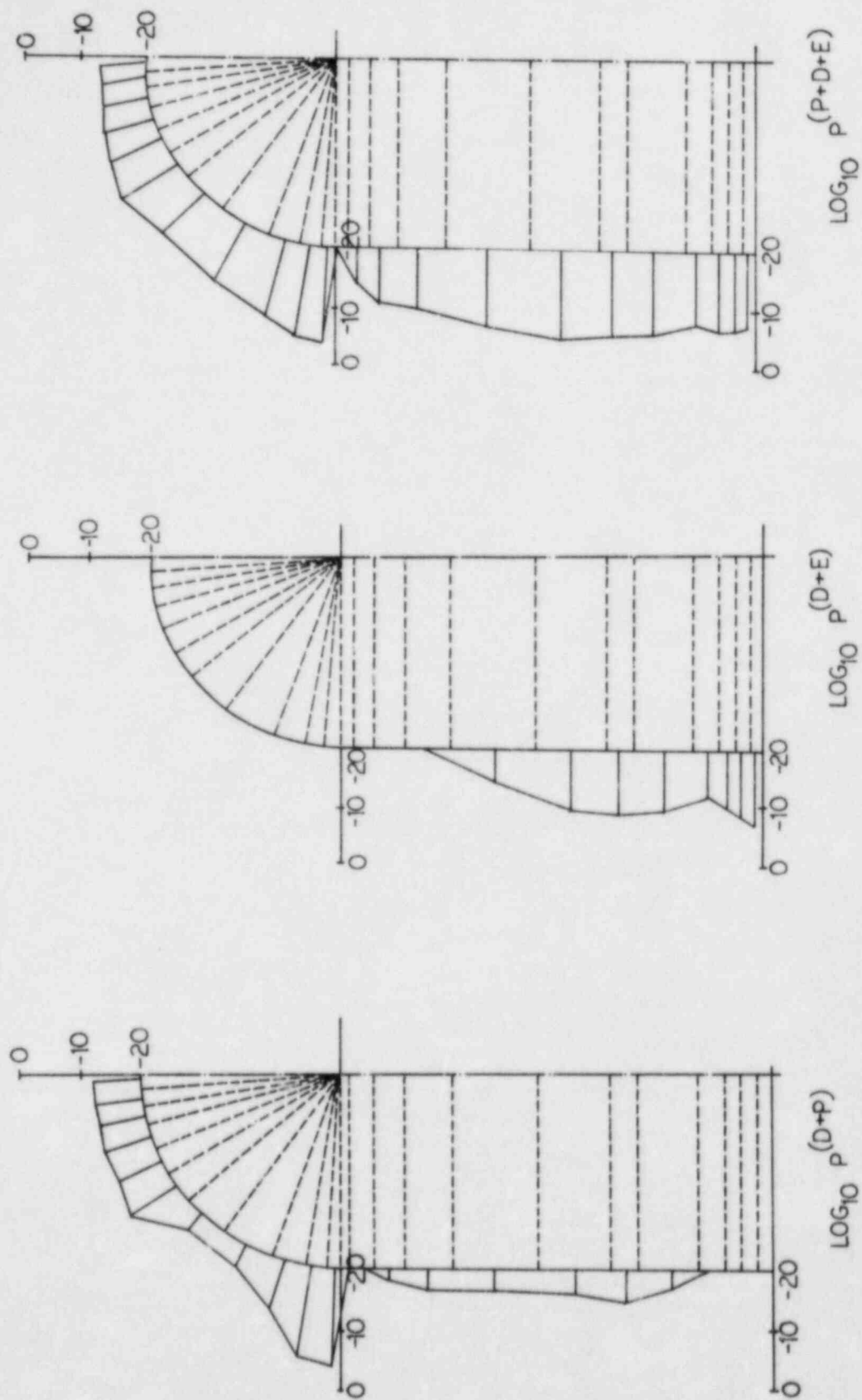


Fig. 14 Conditional Limit State Probability Distributions.

120555078877 1 1ANIRD
US NRC
ADM-DIV OF TIDC
POLICY & PUB MGT BR-PDR NUREG
W-501
WASHINGTON DC 20555